RESEARCH ARTICLE

The influence of pH on the adsorption groups of *Serratia marcescens* for yttrium

Changli Liang[1, 2, *], Jinxi Wang[1], Wenjing Wang[1], Yuhan Yang[1], Jingying Li[1], Xinyu Li[1], Leitong Li[1], Zhi Xu[1], Junhe Liu[1]

[1]School of Biological and Food Processing Engineering, Huanghuai University, Zhumadian, Henan, China. [2]School of Resources and Environmental Engineering, Jiangxi University of Science and Technology, Ganzhou, Jiangxi, China

Received: November 22, 2023; **accepted:** January 12, 2024.

Some groups such as carboxyl, phosphate, and hydroxyl on the surface of adsorbents were considered very vital to recovery rare earth elements (REEs) from wastewater by adsorption, and the main adsorption groups vary with the vary of pH value. The adsorption performance and the groups of *Serratia marcescens* adsorption yttrium (Y(III)) at pH 2.0, 3.5, and 5.5 were studied in the present study. The adsorption capacity of *Serratia marcescens* for Y(III) increased from 26.83 mg/g to 69.19 mg/g with the increase of pH from 2.0 to 5.5. Field emission transmission electron microscope (FETEM) confirmed that Y(III) was adsorbed on the *Serratia marcescens* cell surface, and the adsorption amount increased with the increases of the pH value. Fourier transform infrared spectroscopy (FTIR) and X-ray photoelectron spectroscopy (XPS) results confirmed carboxylate and hydroxy groups mainly complexation with Y(III) at pH 2.0. Y(III) was captured on the *Serratia marcescens* surface under the combined actions of carboxylate and hydroxy and amine groups at pH 3.5 and 5.5, and amine became main adsorption groups at higher pH. The results showed amine, carboxylate, and hydroxy should be the groups of *Serratia marcescens* adsorption for yttrium. The results provided theory foundation for the preparation of high efficiency adsorbents by enhancing the adsorption groups of adsorbents surface through directive chemical modification.

Keywords: *Serratia marcescens;* rare earth elements; adsorption; yttrium; adsorption groups.

[*]**Corresponding author:** Changli Liang, School of Biological and Food Processing Engineering, Huanghuai University, Zhumadian 463000, Henan, China. Email: lclwind@163.com.

Introduction

Rare earth elements (REEs) was termed as the "industrial vitamin" mainly for their excellent optical, electric, and magnetic properties. Wastewater from the addition of REEs in the industrial activities and the production of REEs increase greatly with the growing usage and demand of REEs [1]. REEs has been considered as the hazardous substances in wastewater [2]. Water pollution from REEs wastewater has become a global concern. Some studies found that the exposure to REE caused some diseases such as nephrogenic systemic fibrosis and severe damage on the nephrological system [3-5], dysfunctional neurological disorders [6], and bioaccumulation in brain [7]. Therefore, recovery REEs from the wastewater is urgent for the elimination of its harm to environmental and human health and can resolve the shortness of REEs supply. Currently, the recovery of REEs from wastewater mainly relies the traditional

wastewater treatment methods such as chemical precipitation [8], ultra filtration [9], solvent extraction [10], electrostatic pseudo liquid membrane [11], and adsorption [12]. Biosorption, the adsorption process using biomaterial or biopolymer as adsorbents, mainly includes fungi, bacteria, yeasts, algae, and plant-derived materials [13, 14]. In comparison with traditional methods, biosorption with the advantages of efficient, high selectivity, renewability, low cost, and suitable for treating low concentrations wastewater [15-18]. Biosorption has been considered as one promising method to recover REEs from wastewater.

Some studies showed that the functional groups such as carboxyl, hydroxyl, amine, and phosphoryl on the biosorbents surface were vital to the adsorption capacity of biosorbents adsorption of REEs from wastewater [19, 20]. Kazak *et al*. analyzed adsorption functional groups of *Bacillus subtilis* for europium (Eu(III)) at different pH and found that Eu(III) was mainly complexed with carboxylic groups at pH 5, while Eu(III) mainly complexed with phosphoryl and carboxylic groups at the pH higher than 5 [21]. Ngwenya identified the lanthanides sorption sites on the bacterial surface by analyzing the X-ray absorption spectroscopic (XAS) spectra and found that phosphoryl mainly complexed with light and mostly middle lanthanides (lanthanum to Gdolinium), while some middle and heavy lanthanides (Terbium to Ytterbium) complexed with carboxylate and phosphoryl [22]. Liu *et al*. reported carboxyl, amino, sulfate, and hydroxyl were the adsorption functional groups of *Laminaria ochroleuca* and *Porphyra haitanensis* for REEs [23]. Hosomomi *et al*. found the modification of *E. coli* by diglycolic amic acid increased the maximum adsorption capacity for neodymium (Nd (III)), dysprosium (Dy (III)), and lutecium (Lu (III)) about 2.63, 2.15, and 1.65 times, respectively [24]. Previous studies showed that the adsorption functional groups of biosorbents were mainly responsible for the adsorption capacity of REEs from water and were various with the different adsorption solution pHs.

Serratia marcescens is the biosorbent isolated from the wastewater of a heavy yttrium rare earth mining area in Ganzhou, Jiangxi, China. It demonstrated well adsorption capacities for yttrium and europium in our previous studies [25, 26]. However, the influence of pH on the adsorption functional groups of *S. marcescens* for yttrium was not revealed in the previous studies. The revelation of the adsorption functional groups of *Serratia marcescens* at different pH can provide guidance for the design of *Serratia marcescens* rich in effective adsorption functional groups of yttrium to adapt to the recovery of yttrium in wastewater with different pH. The aim of the present work was to characterize the adsorption functional groups of *S. marcescens* for yttrium at different pH. The adsorption functional groups at different pH were characterized by using Field emission transmission electron microscope (FETEM), Fourier transform infrared spectroscopy (FTIR), and X-ray photoelectron spectroscopy (XPS) spectrum. The results of this study would provide theoretical and technological guidance for the design of efficient biosorbents through directive chemical modification to enhance the biosorbents surface adsorption groups amounts, which could be used in the adsorption recovery yttrium from wastewater.

Materials and Methods

Preparation of *S. marcescens*

S. marcescens used in the work was the same as described in our previous study [25] and domesticated in Y(III) solution. *S. marcescens* were cultured in the liquid beef extract peptone medium and stirred in a rotary shaker at 150 rpm, 37°C for about 48 hours. *S. marcescens* biomass was harvested by centrifuging at 8,000 rpm at 4℃ for 20 minutes. The biomass was then washed three times using deionized water before freezing-dried for future use as biosorbents.

Synthetic yttrium wastewater

Synthetic yttrium solution was prepared by dissolving 0.1 g Y_2O_3 (Bioengineering, Shanghai, China) in 100 mL deionized water and adding 2 mL of 0.1M H_2SO_4. The solution was heated and stirred until completely dissolved. Once the solution was cooled down to room temperature, deionized water was added to bring the total volume to 250 mL. Y(III) solution concentration was measured by using iCAP 7000 Inductively coupled plasma optical emission spectroscopy (ICP-OES) (Thermo Fisher Scientific, Waltham, Massachusetts, USA). Stock Y(III) solutions was stored at 4℃.

Biosorption experiments

Biosorption experiments were conducted by adding 100 mg/L *S. marcescens* into 150 mL Erlenmeyer flask contained 100 mL of 100 mg/L Y(III) solution adjusted to different pH values with 0.1M H_2SO_4 or NaOH solution to 2, 3.5, and 5.5, respectively. The solution was shocked at 150 rpm for 2 h in NHWY-100B constant-temperature oscillator (Baidianyiqi, Shanghai, China) at room temperature. The adsorption capacity of *S. marcescens* for yttrium was calculated as below.

$$\text{Adsorption capacity} = (C_0 - C_e) \times \frac{V}{m} \quad (1)$$

where C_0 and C_e were the initial and equilibrium concentrations of Y(III) (mg/L), respectively. m was the mass of the adsorbent (g). V was the volume of Y(III) solution (L). All experiments were conducted in independent triplicates.

Characterization

Biomass analyzed by FETEM was mainly prepared through the following procedures. Briefly, *S. marcescens* before and after Y(III) biosorption were fixed with glutaraldehyde before washed with cacodylate. The samples were dehydrated with graded ethanol and then resin embedded. Samples were analyzed using Tecnai G2 F30 FETEM (FEI Company, Hillsboro, Oregon, USA) equipped with Xplore 30 Energy dispersion spectrometer (EDS) (Oxford instruments, Oxford, UK). Infrared spectra of *S. marcescens* before and after adsorption Y (III) were recorded in the range of 4,000 – 800/cm using Nicolet 5 Fourier transform infrared spectrophotometer (Thermo Fisher Scientific, Waltham, Massachusetts, USA). High-resolution C 1s, N 1s, O 1s P 2p and Y 3d XPS spectra of *S. marcescens* before and after Y (III) biosorption were recorded using Escalab 250XI X-ray photoelectron spectrometer (Thermo Fisher Scientific, Waltham, Massachusetts, USA). Spectra were fitted and analyzed using Thermo Advantage11 software (Thermo Fisher Scientific, Waltham, Massachusetts, USA).

Statistical analysis

Origin 8 (OriginLab Corporation, Northampton, Massachusetts, USA) was employed for the statistical analysis of this study. The results were presented as the mean values of triplicated experiments under identical conditions.

Results and discussion

Adsorption behaviors

The adsorption capacity of *S. marcescens* for Y(III) increased with the increase of pH in the three studied pH values. The adsorption capacities at pH 2.0, 3.5, and 5.5 were 26.83, 40.23, and 69.19 mg/g, respectively (Figure 1). The influence of pH on the adsorption capacity was consistent with some studies [27-29]. Palmieri *et al*. also found that the adsorption capacity of *Sargassum fluitans* for lanthanum kept increasing with the increase of pH, and the q_{max} increased from 0.049 mmol/g to 0.53 mmol/g with the pH increased from 2 to 5. The poor adsorption performance of *S. marcescens* for Y(III) at pH 2.0 and 3.5 should mainly be resulted from the competing for the H^+ with Y(III) on the surface of cell and the positive charge because the pH lower than its isoelectric point 4.47 [28].

Characterization of adsorption sites by FETEM

Biosorbents can adsorb REEs on their surface, and/or bioaccumulate them inside the cell. The morphology and elemental composition of *S. marcescens* before and after adsorbed Y(III) under different pHs were analyzed using FETEM

Table1. Elemental composition of raw *S. marcescens* and *S. marcescens* adsorbed Y(III) under different pH values by using EDS.

Elemental composition（%）	C	N	O	P	Y
Raw *S. marcescens*	83.43	6.41	9.84	0.32	
Adsorption Y(III) at pH 2.0	84.43	5.43	9.44	0.47	0.23
Adsorption Y(III) at pH 3.5	84.67	4.19	10.21	0.5	0.43
Adsorption Y(III) at pH 5.5	80.09	6.94	10.43	1.57	0.97

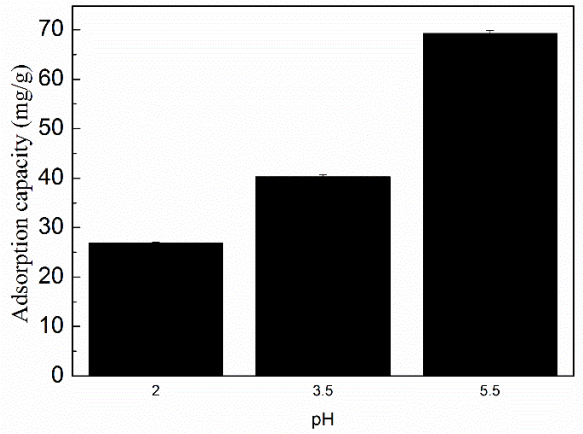

Figure 1. Influence of pH on the adsorption capacity of *S. marcescens* for Y(III).

equipped with EDS to determine the sites that Y(III) was adsorbed on the *S. marcescens* cell. The raw *S. marcescens* demonstrated distinct cell borders and some inclusion particles inside the cells. There were no distinct differences being observed among the cell micrographs of *S. marcescens* before and after adsorption of Y(III) (Figure 2). However, some black particles were found at the outside of the cell borders in the FITEM micrographs of adsorbed yttrium, and the amounts of them increased with the increase of pH. The elemental composition of *S. marcescens* before and after adsorption of Y(III) was shown in Table 1. The results confirmed the yttrium on the cell surface of *S. marcescens*, and yttrium elemental content on the cell surface increased from 0.23% to 0.97% with the pH increased from 2.0 to 5.5. The EDS analysis was consistent with the adsorption behaviors of *S. marcescens* for Y(III) under different pH.

FTIR characterization

It has been reported that some groups on the surface of biosorbents are very vital to their adsorption capacity for heavy metals from wastewater, and the adsorption functional groups vary with the various of the pH of adsorption solution [28, 29]. To characterize the adsorption functional groups of *S. marcescens* for Y(III) at different pH values, the FTIR spectra of *S. marcescens* before and after adsorbed Y(III) at different pHs, and the spectra of raw *S. marcescens* at three pH values were recorded (Figure 3). The results showed that the broad peak centered in the range of 3,426 to 3,443/cm. A shoulder peak at 3,295/cm could be allocated to the overlapped stretching vibrations in the hydroxyl (–OH) and amine ($–NH_2$) groups derived from the sugars and amino acids [19, 30, 31]. The peak neared 1,650/cm could be attributed to the overlapping of the asymmetric stretching vibration of carboxylate and amine I [27, 32, 33]. The peak near 1,540/cm should be attributed to the stretching vibration of carboxylate anion [34]. The double peaks near 1,455/cm and 1,400/cm should be resulted from the stretching vibrations of carboxyl anion and C–O and the deformation vibration of the O–H in the carboxyl groups [27, 35]. In addition, the asymmetric stretching of phosphodiester P=O and stretching vibrations of C–OH were recorded at about 1,237/cm and 1,074/cm, respectively [36, 37]. The FTIR spectra of raw *S. marcescens* at different pHs were shown in Figure 3a. There were some distinct differences among the FTIR spectra of pH 2.0, 3.5, and 5.5. In the FTIR spectra of pH 5.5, the amine shoulder peak negatively shifted to 3,282/cm and the amine peak positively shifted to 1,647/cm. The differences of the amine peaks at pH 5.5 should be resulted from the weakening of protonation of $–NH_2$ to $–NH_3^+$ because pH 5.5 was higher than the isoelectric point of *S. marcescens*

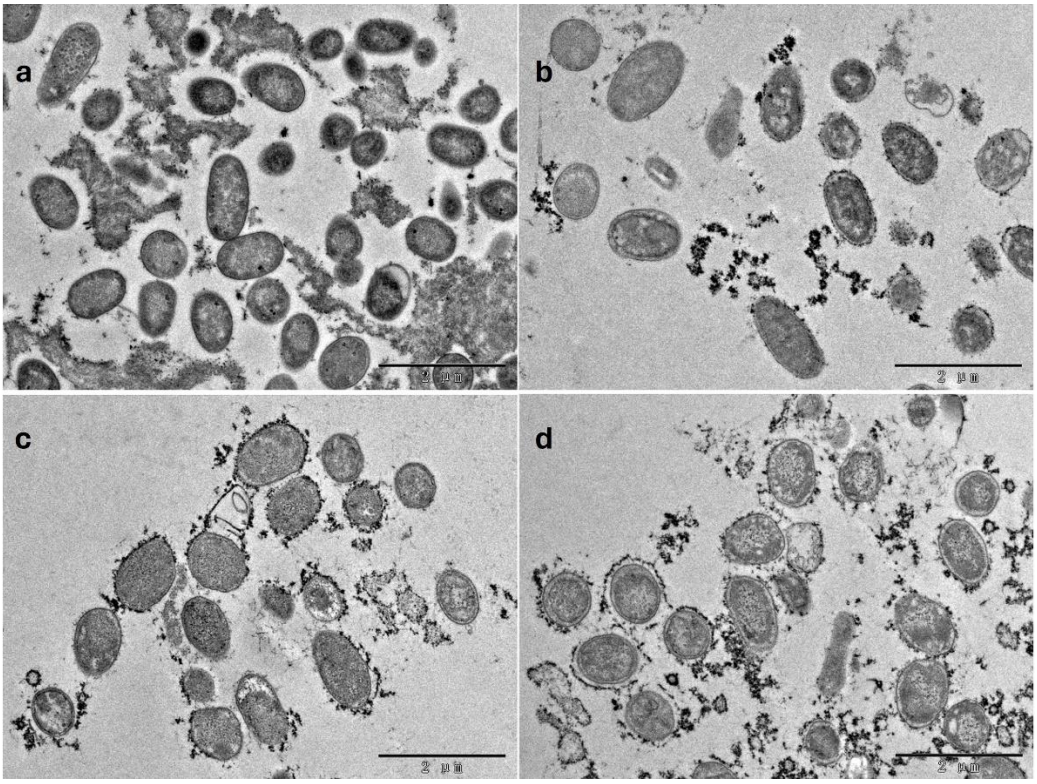

Figure 2. FITEM micrographs of *S. marcescens*. **a:** raw *S. marcescens*. **b, c, and d:** *S. marcescens* adsorption of Y(III) at pH 2, 3.5, and 5.5, respectively.

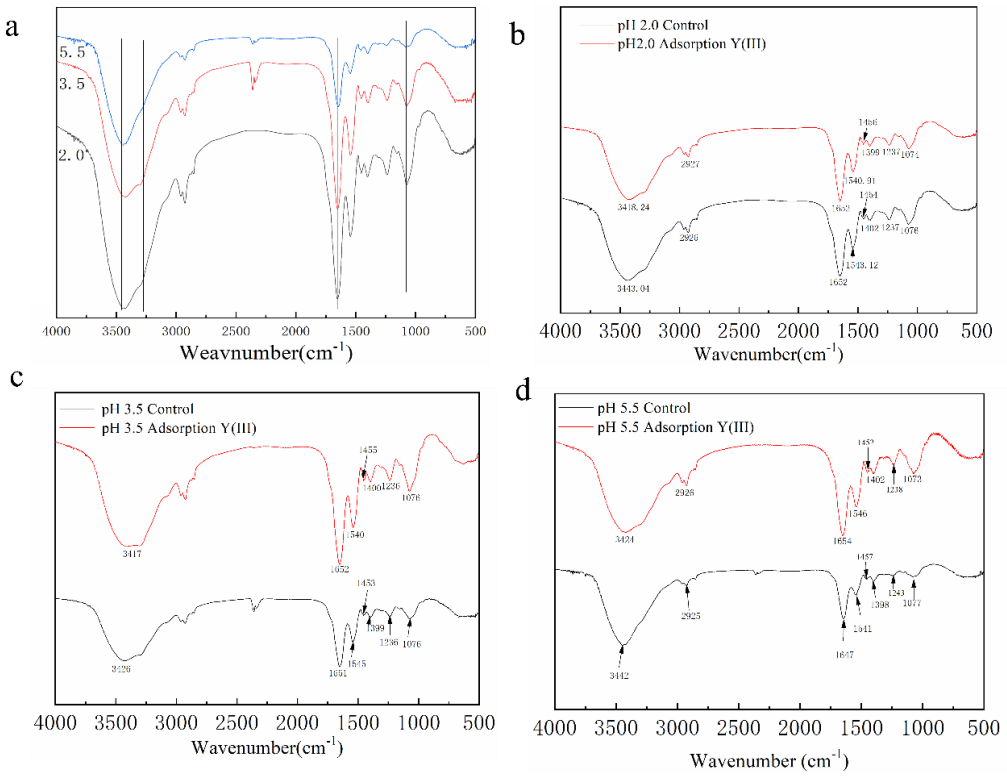

Figure 3. FTIR spectra of raw *S. marcescens* at different pH (a) and *S. marcescens* before and after adsorbed Y(III) at pH 2.0 (b), 3.5(c), and 5.5(d).

[28, 38, 39]. The stretching vibrations peak of C–OH at 1,077/cm was found broaden at pH 5.5 in comparison with that of pH 2.0 and 3.5, which indicated the different dissociation of phosphodiester P=O. The analysis of the FTIR spectra of raw *S. marcescens* at three pH values confirmed that the dissociation of surface groups varies with the various of pH [38]. Slight differences were found between the FTIR spectrum of *S. marcescens* before and after adsorbed Y(III) at pH 2.0. No distinct differences were found at the shoulder peak of $–NH_3^+$ group at 3,295/cm and the amine groups at 1,652/cm after adsorbed Y(III). The peak of hydroxyl groups shifted from 3,443.04/cm to 3,418.24/cm after adsorbed Y(III) indicated the involvement of hydroxyl groups in the adsorption. The analysis of the FTIR spectrum of *S. marcescens* before and after adsorbed Y(III) at pH 2.0 indicated that the hydroxy of alcohol and/or carboxy groups on the surface of *S. marcescens* should mainly be responsible for the adsorption of Y(III). The peaks of hydroxyl and amine groups negatively shifted from 3,426/cm to 3,418/cm along with the flatten of amine shoulder peak after adsorbed Y(III) at pH 3.5, which indicated that the involvement of $-NH_2$ was enhanced because the weaken of amine groups protonation when the pH increased to 3.5. The peak at 1,545/cm shifted to 1,540/cm and the peak intensity was strengthened after adsorbed Y(III), indicated the complexation of carboxyl group with Y(III). The strength of phosphodiester groups at 1,076/cm resulted from the complexation of PO_4^{-3} with Y(III). The analysis of the FTIR spectra of *S. marcescens* before and after adsorbed Y(III) confirmed the carboxyl, phosphodiester, hydroxyl, and amine groups complexation with Y(III) at pH 3.5. Some distinct differences were observed in the spectra of *S. marcescens* before and after adsorbed Y(III) (Figure 3d). The negative shift of the peak for hydroxyl and amine groups from 3,442/cm to 3,424/cm and some changes of the shoulder peak were observed after adsorption, which indicated the interactions of Y(III) with hydroxy and amine groups. The peak at 1,647/cm positively shifted to 1,654/cm and the enhancement of peak intensity indicated the complexation of amine group with Y(III). The peak at 1,541/cm positively shifted to 1,546/cm along with the increase of the peak intensity, which should be resulted from the complexation of the carboxylate anion group with Y(III) [34]. The peaks appeared at 1,243/cm and 1,077/cm were both enhanced after adsorbed Y(III), which indicated the phosphodiester and C–OH groups interacting with Y(III). The analysis of the FTIR spectra of *S. marcescens* adsorption of Y(III) at pH 5.5 indicated that the carboxylate, hydroxy, phosphodiester, and amine groups should be responsible for the adsorption of Y(III), and the contribution of amine was enhanced. The analysis of the FTIR spectra of *S. marcescens* before and after adsorbed Y(III) at different pH confirmed that the groups involvement in the adsorption varied with the different pH values [28, 29, 38].

XPS characterization

To further reveal the influence of pH on the adsorption groups of *S. marcescens* for Y(III), *S. marcescens* before and after adsorbed Y(III) at the three pH values were analyzed using XPS. The C1s XPS peak could be deconvoluted to the peaks at 284.5 eV, 285.9 eV, and 287.6 eV, and be assigned to -C-C/C-H, -C-O/C-N, and -C=O groups which derived from the sugars, alcohols, polysaccharides, and protein of *S. marcescens*, respectively [40] (Figure 4a). The peak appeared at 399.6 eV and 401.3 eV in the N 1s deconvolution spectra of raw *S. marcescens* could be assigned to -N-C=O/NH_2 and $-NH_3^+$ derived from protein and oxidation states of N atoms with positively charged $R-NH_3^+$, respectively [30] (Figure 4b). Peaks with binding energy of 531.2 eV, 532.4 eV, and 534.1 eV in the O 1s deconvolution spectra of raw *S. marcescens* could be respectively allocated to the –OH, C=O/C–O, and COO− groups, which were derived from sugars, amino acids, and ether [31] (Figure 4c). The P 2p spectra of raw *S. marcescens* could be fitted to two doublets of $PO_4^{3-}{}_{2p3}$ at 133.1 eV and $PO_4^{3-}{}_{2p1}$ at 134.2 eV derived of the spin-orbit components, and the ratio of it was about 2:1 and a separation of 1.1 eV [39] (Figure 4d).

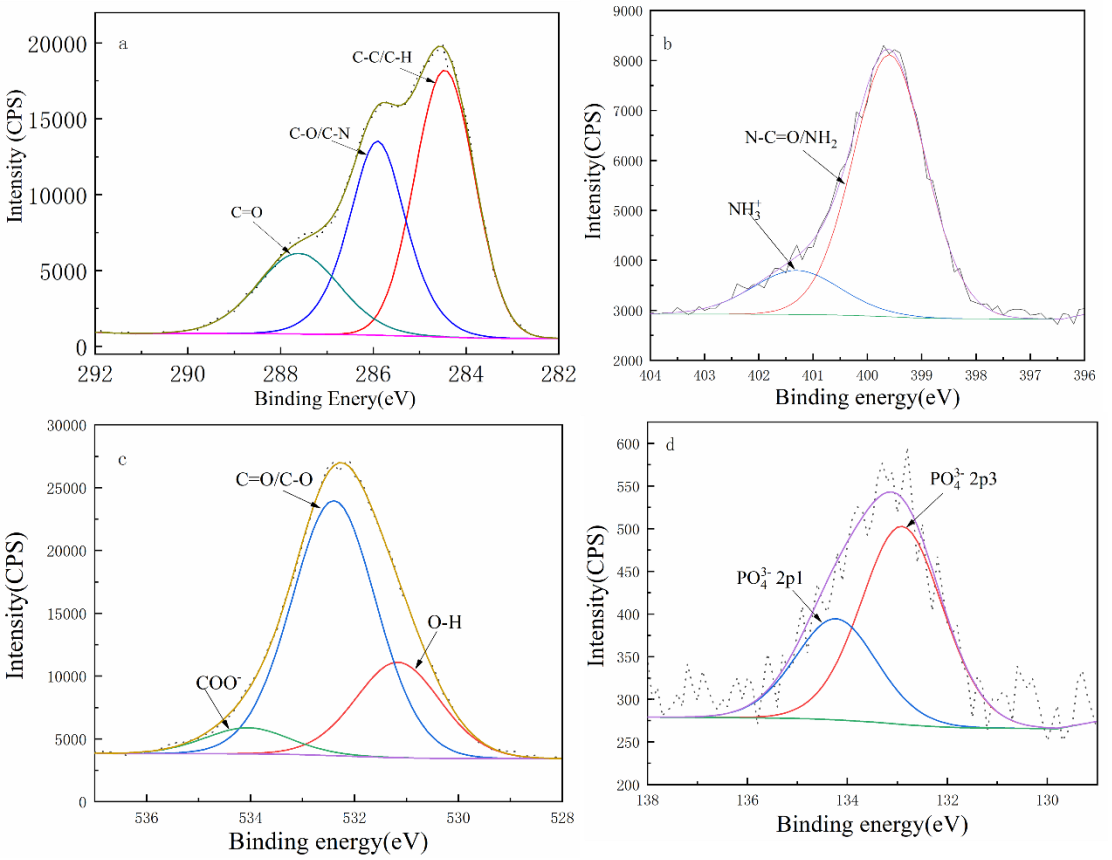

Figure 4. XPS spectra of raw *S. marcescens* at pH 2.0. **a.** C1s spectra. **b.** N1s spectra. **c.** O1s spectra. **d.** P2p spectra.

Table 2. Elemental composition of *S. marcescens* before and after adsorbed Y(III) at different pH.

Atomic concentration (AC%)	C	N	O	P	Y
Control at pH 2.0	65.9	8.06	25.28	0.75	
Adsorption Y(III) at pH 2.0	65.45	7.31	26.47	0.62	0.15
Control at pH 3.5	65.14	8.03	26.16	0.67	
Adsorption Y(III) at pH 3.5	64.81	7.35	26.84	0.68	0.32
Control at pH 5.5	65.29	7.38	26.76	0.56	
Adsorption Y(III) at pH 5.5	62.75	7.14	27.79	0.59	1.73

The main photoelectron peaks at 132.82 eV, 284.83 eV, 399.62 eV, and 532.22 eV in the survey XPS spectra of raw *S. marcescens* at pH 2.0 could be allocated to P(2p), C(1s), N(1s), and O(1s), respectively (Figure 5a). In comparation with raw *S. marcescens*, a weak photoelectron peak of Y(3d) was observed in the survey spectrum of *S. marcescens* adsorbed Y(III). The yttrium accounted for 0.15 AC% of the cell surface (Table 2) confirmed that the adsorption of Y(III) at pH 2.0 was weak. In comparation of the C1s and N 1s spectra of *S. marcescens* before and after adsorbed Y(III), no obvious varies of peak shape and binding energy were found between before and after adsorption (Figures 4a, 4b, 5b, 5c). A new peak of -O-H/Y-O was observed at 531 eV and the binding energy of C=O/C-O peak positively shifted for 0.5 eV after adsorption (Figure 5d). The formation of Y-O indicated -OH groups in the carboxyl and alcohols complexation

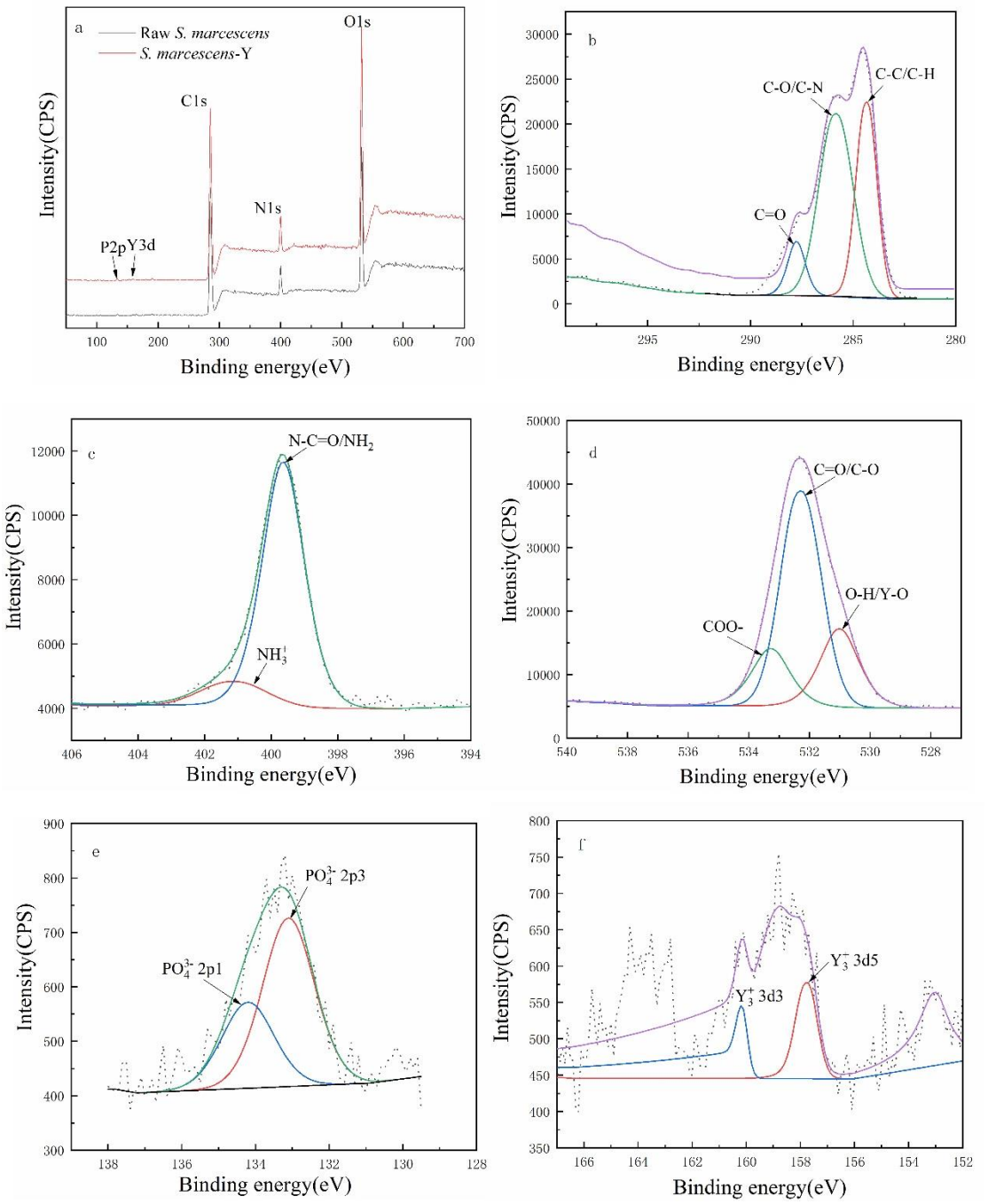

Figure 5. XPS spectra of *S. marcescens* adsorption of Y(III) at pH 2.0. Survey spectra of *S. marcescens* before and after Y(III) biosorption (**a**), C1s spectra (**b**), N1s spectra (**c**), O1s spectra (d), P2p spectra (**e**), and Y3d spectra (**f**).

with Y(III) and the involvement of -OH and C=O/C-O groups in the adsorption of Y(III). Y 3d spectra analysis confirmed that yttrium was adsorbed as trivalent ion, and no redox reactions took place during the adsorption. The results confirmed that *S. marcescens* adsorption Y(III) at pH 2.0 was weak, and -OH groups were the main adsorption active groups.

Compared to pH 2.0, the contents of C, N, and P all decreased, and the content of O increased at pH 3.5 (Table 2). The differences of the elemental

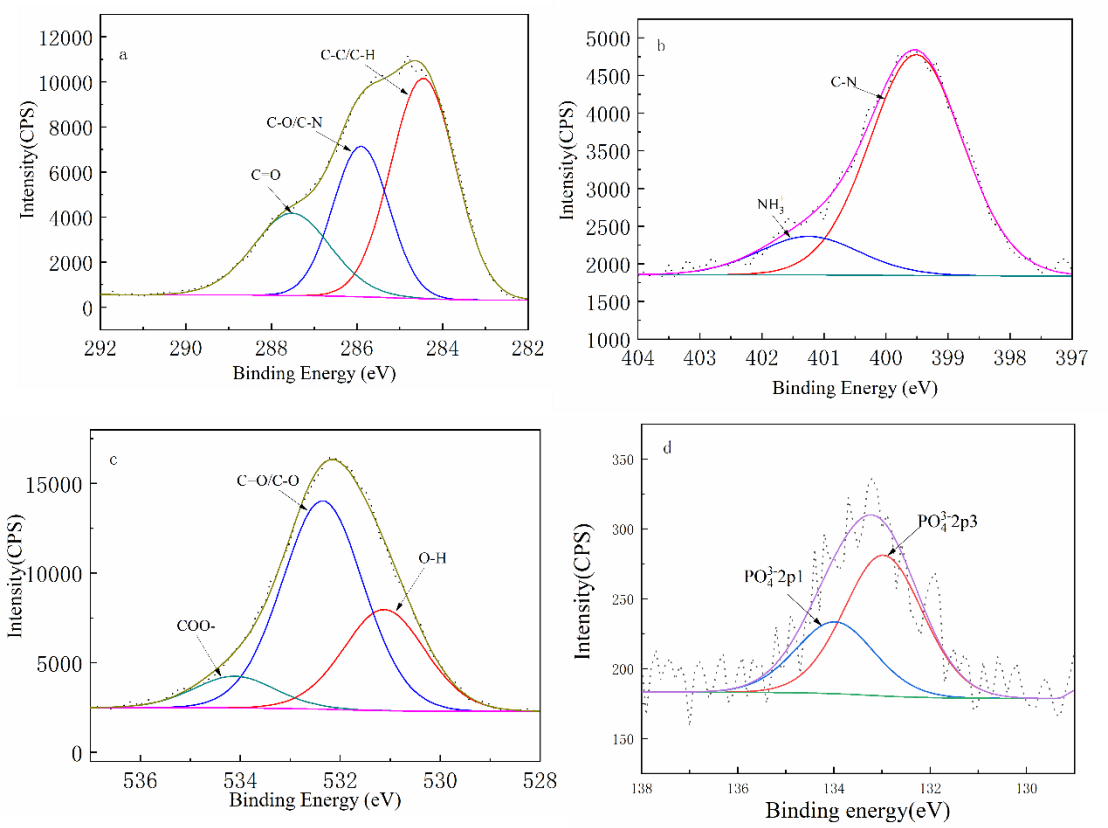

Figure 6. XPS spectra of raw *S. marcescens* at pH 3.5. C1s spectra (**a**), N1s spectra (**b**), O1s spectra (**c**), and P2p spectra (**d**).

composition of raw *S. marcescens* cell surface at different pH should be resulted from the dissociation of cell surface groups various with the different pHs [30]. Some distinct differences of peaks shape were found between the C 1s high-resolution spectra of *S. marcescens* before and after adsorbed Y(III) at pH 3.5 (Figures 6a and 7b). The platform at 287.7 to 287.3 eV and 285.8 to 285.3 eV became more distinct along with the enhanced peak intensity (Figure 7d). The content of $-NH_3^+$ on the surface of raw *S. marcescens* decreased from 17.04 AC% to 15.87 AC% with the pH increased from 2.0 to 3.5, which might be due to the weakening of protonation of $–NH_2$ to $–NH_3^+$ with the increase of pH [28]. In the N 1s spectra, a new peak appeared at 401.7 eV, indicating the complexation of Y(III) with $–NH_2$ group. The increase of binding energy of N–Y(III) should be resulted from the reduction of the electron cloud density of nitrogen atoms for complexation with yttrium atoms [41]. One distinct characteristic peak of yttrium was observed at 158.12 eV in the survey spectra of *S. marcescens* adsorbed Y(III) at pH 3.5 (Figure 7a), which accounted for 0.32 AC% of the cell surface (Table 2). The results confirmed that the adsorption of Y(III) at pH 3.5 was enhanced compared to that of pH 2.0. O 1s deconvolution spectra of *S. marcescens* adsorbed Y(III) at pH 3.5 contained –O–H/Y–O, –C=O/C–O, and $–COO^-$ groups at 530.9 eV, 532.3 eV, and 533.2 eV, respectively. The increase of oxygen AC% from 26.16% to 28.84% and the arisen of –Y–O peak resulted from the complexation of Y(III) with –C=O and –OH groups [42] (Figure 7e). P 2p spectra showed that there were no obvious changes of binding energy and peak shapes after adsorption (Figures 6c and 7e), and phosphorus atoms remained existed as PO_4^{3-}. The appearance of –Y–O $_{3d/2\text{-}5d/2}$ double peaks after adsorption confirmed the complexation of –OH with Y(III) at pH 3.5 (Figure 7f). The analysis of the XPS spectra

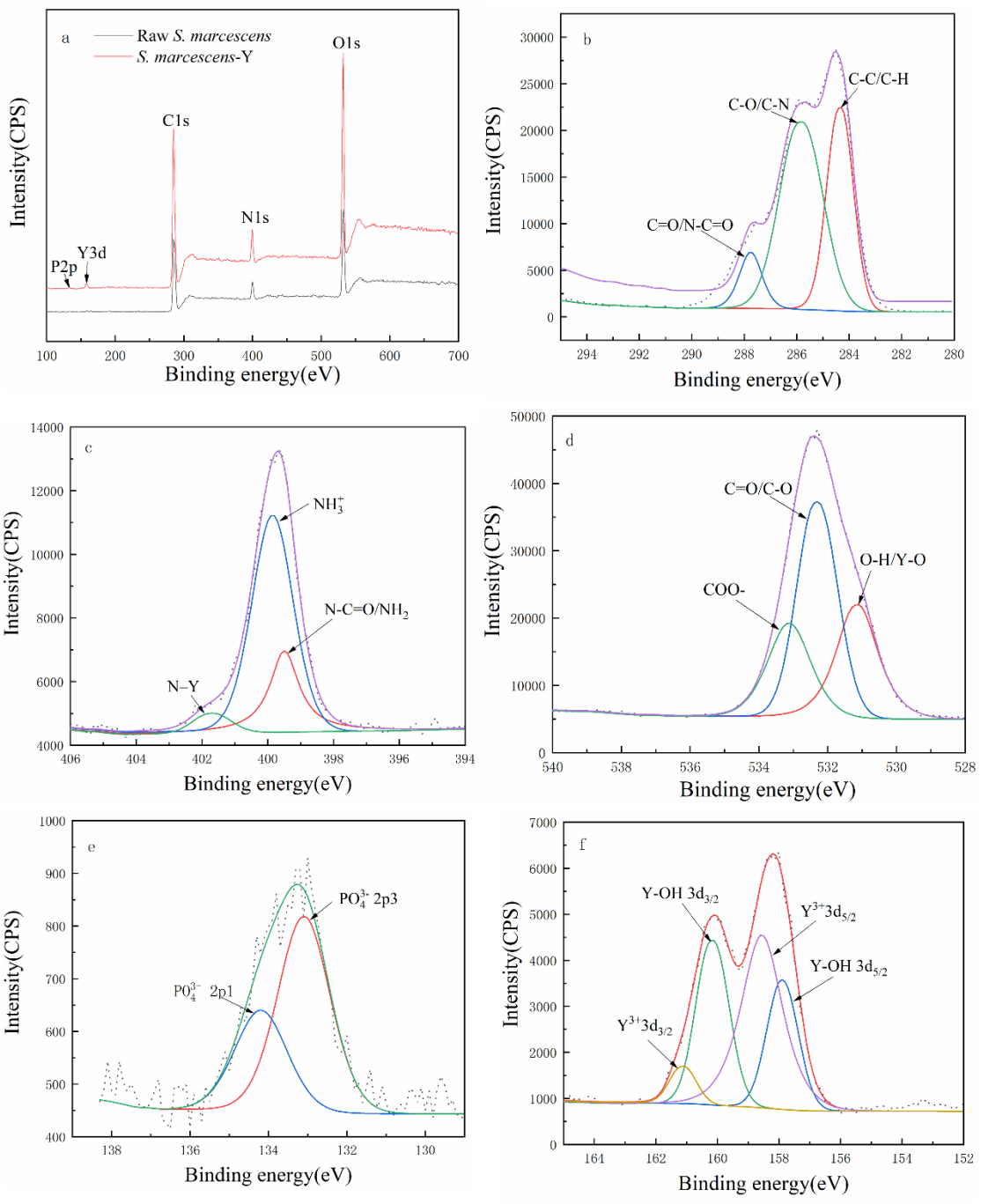

Figure 7. XPS spectra of *S. marcescens* adsorption of Y(III) at pH 3.5. Survey spectra of *S. marcescens* before and after Y(III) biosorption (**a**), C1s spectra (**b**), N1s spectra (**c**), O1s spectra (**d**), P2p spectra (**e**), and Y3d spectra (**f**).

of *S. marcescens* before and after adsorbed Y(III) at pH 3.5 indicated that the –C=O and –OH groups derived from alcohol and carboxyl acid and nitrogen groups $–NH_2$ derived from the protein should complex with Y(III) during the adsorption. Some obvious differences were found between the C1s spectra of *S. marcescens* before and after adsorbed Y(III) at pH 5.5 along with the increase of the peak intensity (Figures 8a and 9b). The adsorption peak with the binding

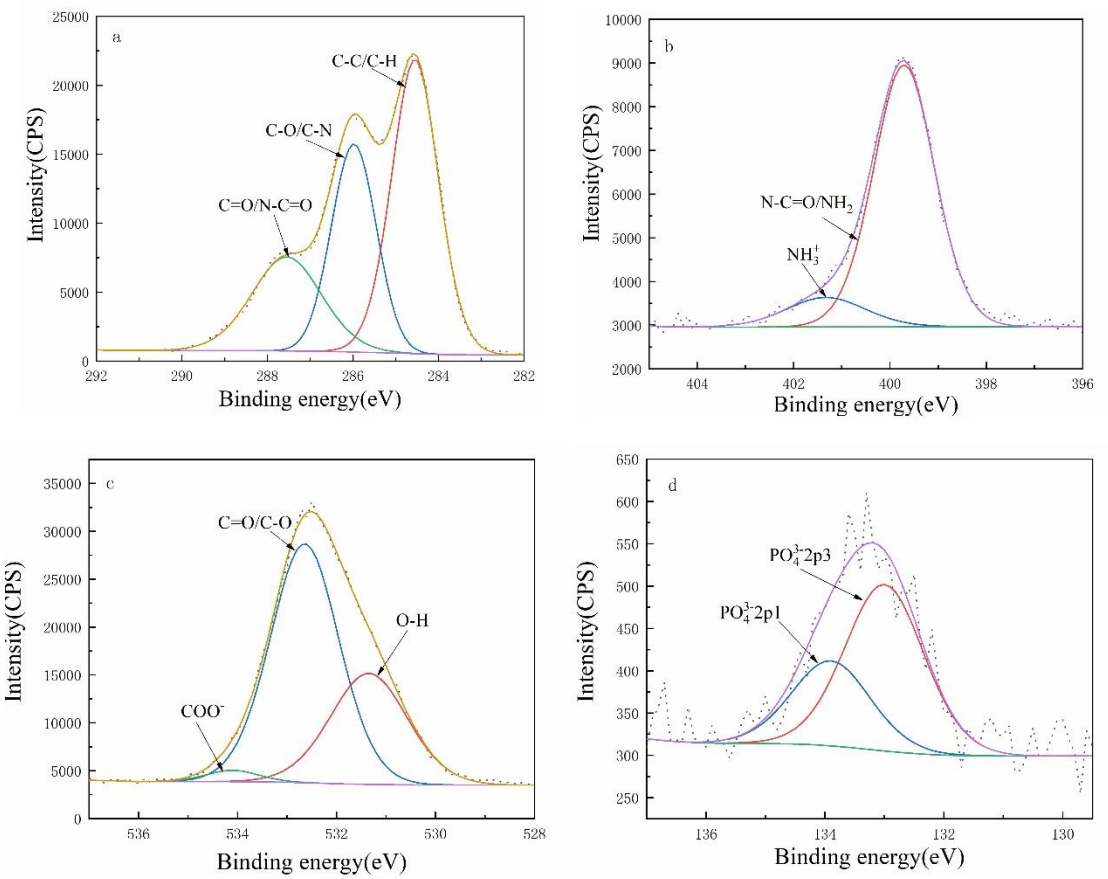

Figure 8. XPS spectra of raw *S. marcescens* at pH 5.5. C1s spectra (**a**), N1s spectra (**b**), O1s spectra (**c**), and P2p spectra (**d**).

energy of 286.5 eV to 286 eV became more plate after adsorbed Y(III). The deconvoluted peaks of C1s spectra showed 4 peaks of carbon atoms groups and the contents changed after adsorbed of Y(III). The analysis of C1s spectra confirmed the involvement of carboxyl in the adsorption of Y(III). A more distinct characteristic peak for yttrium was observed in the survey spectra of pH 5.5 (Figure 9a), and it accounted for 1.73 AC% of the cell surface (Table 2). The results were consistent with the results of adsorption experiments, which confirmed that the adsorption of *S. marcescens* for Y(III) at pH 5.5 was far higher than that of pH 3.5 and 2.0. One new peak with binding energy of 400.4 eV was found after adsorbed Y(III) (Figures 8b and 9c), and it could be allocated to N–Y group. The peaks at 399.7 eV and 401.3 eV negatively shifted to 399.3 eV and 399.9 eV after adsorption, respectively. The formation of peak N–Y and the shift of $–NH_2$ resulted from the complexation of $–NH_2$ groups with Y(III). The peak content of N–Y of pH 5.5 was far higher than that of pH 3.5 (Figures 7c and 9c), which indicated that the contribution of $–NH_2$ group became more important at pH 5.5. The convoluted peaks of O1s spectra of *S. marcescens* adsorbed Y(III) became obvious widen (Figures 8c and 9d). Meanwhile, the peaks of –C=O and $–COO^-$ groups negatively shifted after adsorption. The appearance of the new peak at 531.3 eV was assigned to the formation of Y–O by –OH groups complex with Y(III) [42, 43]. The results indicated the -OH in the alcohol/carboxyl complex with Y(III). No obvious differences on peak shape were observed between the P 2p spectra of *S. marcescens* before and after adsorbed Y(III) at pH 5.5. Slightly positive shift of binding energy and the increase of phosphorus element content on the cell surface (Table 2) indicated that the phosphate

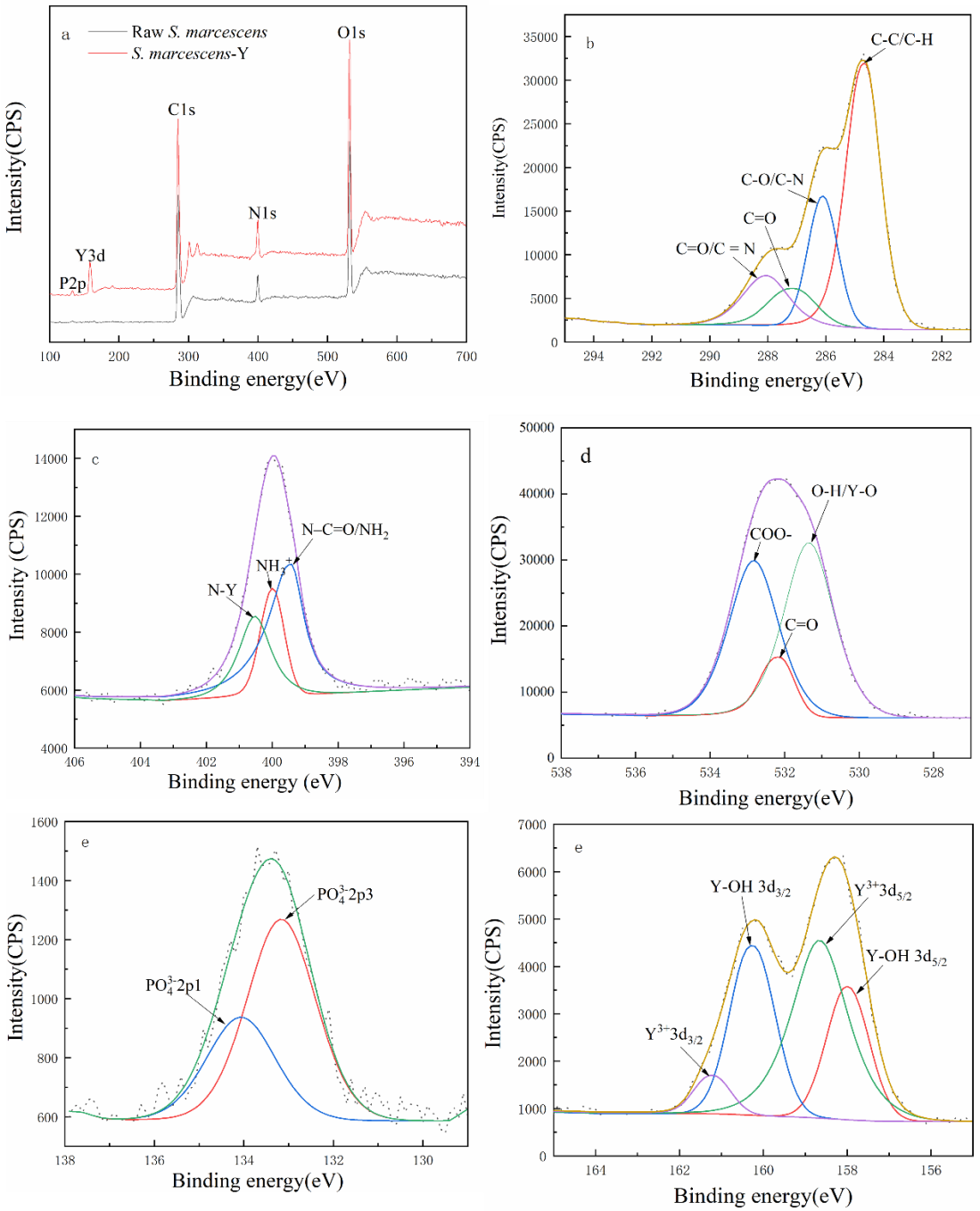

Figure 9. XPS spectra of *S. marcescens* adsorption of Y(III) at pH 5.5. Survey spectra of *S. marcescens* before and after Y(III) biosorption (**a**), C1s spectra (**b**), N1s spectra (**c**), O1s spectra (**d**), P2p spectra (**e**), and Y3d spectra (**f**).

groups might complexation with Y(III). Peaks at 157.9 eV and 160.1 eV could be allocated to the Y $3d_{5/2–3/2}$ doublet of Y–OH group [43], which accounted for 67.5 AC% of yttrium (Figure 9f). The peaks with binding energy of 158.7 eV and 161.2 eV should be the doublet of $Y3d_{5/2–3/2}$ of Y(III) [42-44], which accounted for 31.5 AC%. The results confirmed that the hydroxyl, carboxyl, amine, and phosphate groups on the surface of *S. marcescens* should mainly be responsible for the adsorption of Y(III) at pH 5.5.

The analysis of the high resolution XPS spectra of *S. marcescens* adsorbed Y(III) at pH 2.0, 3.5, and 5.5 showed that the adsorption groups for yttrium ions varied with the different solution pHs, where the –OH groups derived from hydroxyl and/or carboxyl groups mainly complex with Y(III) at pH 2.0, –C=O, –OH, and $–NH_2$ groups mainly responsible for the adsorption of Y(III) at pH 3.5, while the adsorption of Y(III) were under the combine action of –C=O, –OH, PO_4^{3-}, and $–NH_2$ groups at pH 5.5.

Conclusion

The adsorption behaviors of *S. marcescens* for Y(III) at pH 2.0, 3.5, and 5.5 showed that the adsorption capacity increased with the increase of pH. The poor adsorption performance at lower pH should be mainly because the electrostatic repulsive action resulted from the protonation of $–NH_3^+$ groups for the pH lower than its isoelectric point and the competing adsorption of H^+ with Y(III). FETEM analysis confirmed that the yttrium was adsorbed on the cell surface at three pH values. FTIR analysis indicated that the carboxylate, hydroxy, phosphodiester, and amine groups should be responsible for the adsorption of Y(III) at pH 5.5, while carboxylate and hydroxy were the main groups adsorption Y(III) at lower pH value. XPS analysis confirmed that hydroxyl and carboxyl groups mainly complexed with Y(III) at pH 2.0, while Y(III) was adsorbed on the cell surface under the combined action of hydroxy, phosphodiester, and amine groups at pH 3.5 and 5.5. The results provided theory for the development of effectively adsorbents for yttrium through directional enhancement of the adsorption groups on the surface of adsorbents by chemical modification.

Acknowledgements

This study was financially supported by the Foundation of the National Natural Science Foundation of China (No. 51964020), The Key Specialized Research and Development Breakthrough Program in Henan province, China (No. 232102111019), and the Primary Research & Development Plan of Henan province, China (No. 231111320300).

References

1. Pereao O, Bode-Aluko C, Fatoba O, Laatikainen K, Petrik LJD. 2018. Rare earth elements removal techniques from water/wastewater: A review. Deaslin Water Treat. 130:71-86.
2. Shin SH, Kim HO, Rim KT. 2019. Worker safety in the rare earth elements recycling process from the review of toxicity and issues. Saf Health Work. 10(4):409-419.
3. Thomsen HS. 2017. Are the increasing amounts of gadolinium in surface and tap water dangerous. Acta Radiol. 58(3):259-263.
4. Ranga A, Agarwal Y, Garg K. 2017. Gadolinium based contrast agents in current practice: Risks of accumulation and toxicity in patients with normal renal function. Indian J Radiol Imag. 27(2):141-147.
5. Pagano G, Guida M, Tommasi F, Oral R. 2015. Health effects and toxicity mechanisms of rare earth elements—Knowledge gaps and research prospects. Ecotox Environ Safe.115:40-48.
6. Zhu WF, Xu SQ, Zhang H, Shao PP, Feng J. 1996. Investigation of children intelligence quotient in REE mining area: Bio-effect study of REE mining area in South Jiangxi. Chinese Sci Bull. 41:914-916.
7. Kanda T, Nakai Y, Hagiwara A, Oba H, Toyoda K, Furui S. 2017. Distribution and chemical forms of gadolinium in the brain: a review. Brit J Radiol. 90:20170115.
8. Chen T, Liu Y, Wei J, Li LZ, Scheckel KG, Luo YM. 2018. Characterization and mechanism of copper biosorption by a highly copper-resistant fungal strain isolated from copper-polluted acidic orchard soil. Environ Sci Pollut R. 25:24965–24974.
9. Park JH, Hyo-Taek C. 2016. Characterization of cadmium biosorption by *Exiguobacterium* sp. isolated from farmland soil near Cu-Pb-Zn mine. Environ Sci Pollut R. 23: 1814–11822.
10. Dong L, Jin Y, Song T, Liang J, Bai X, Yu S, *et al*. 2017. Removal of Cr(VI) by surfactant modified *Auricularia auricula* spent substrate: biosorption condition and mechanism. Environ Sci Pollut R. 24:17626–17641.
11. Gurgel LV, Júnior OK, Gil RP, Gil LF. 2008. Adsorption of Cu(II), Cd(II), and Pb(II) from aqueous single metal solutions by cellulose and mercerized cellulose chemically modified with succinic anhydride. Bioresource Technol. 74(4):922-929.
12. Kucuker MA, Wieczorek N, Kuchta K, Copty NK. 2017. Biosorption of neodymium on *Chlorella vulgaris* in aqueous solution obtained from hard disk drive magnets. Plos One. 12(4):0175255.
13. Vijayaraghavan K, Yun YS. 2008. Bacterial biosorbents and biosorption. Biotechnol Adv. 26(3):266–291.
14. Hansda A, Kumar V, Anshumali. 2016. A comparative review towards potential of microbial cells for heavy metal removal

with emphasis on biosorption and bioaccumulation. World J Microbiol Biotechnol. 32:170.
15. Han Q, Du M, Guan Y, Luo G, Ji Y. 2020. Removal of simulated radioactive cerium (III) based on innovative magnetic trioctylamine-polystyrene composite microspheres. Chem Phys Lett. 741:137092.
16. Anastopoulos I, Bhatnagar A, Lima EC. 2016. Adsorption of rare earth metals: A review of recent literature. J Mol Liq. 221:954–962.
17. Giese EC. 2020. Biosorption as green technology for the recovery and separation of rare earth elements. World J Microb Biot. 36:52.
18. Cao Y, Shao P, Chen Y, Zhou X, Luo X. 2021. A critical review of the recovery of rare earth elements from wastewater by algae for resources recycling technologies. Resour Conserv Recy. 169(6):105519.
19. Cid HA, Flores MI, Pizarro JF, Castillo XA, Barros DE, Moreno-Piraján JC, *et al*. 2018. Mechanisms of Cu^{2+} biosorption on *Lessonia nigrescens* dead biomass: functional groups interactions and morphological characterization. J Environ Chem Eng. 6(2):2696-2704.
20. Moriwaki H, Koide R, Yoshikawa R, Warabino Y, Yamamoto H. 2013. Adsorption of rare earth ions onto the cell walls of wild-type and lipoteichoic acid-defective strains of *Bacillus subtilis*. Appl Microbiol Biot. 97(8):3721-3728.
21. Kazak ES, Kalitina EG, Kharitonova NA, Chelnokov GA, Elovskii EV, Bragin IV. 2018. Biosorption of rare-earth elements and yttrium by heterotrophic bacteria in an aqueous environment. Moscow Univ Geol Bull. 73(3):287-294.
22. Ngwenya BT, Magennis M, Olive V, Mosselmans J, Ellam RM. 2010. Discrete site surface complexation constants for lanthanide adsorption to bacteria as determined by experiments and linear free energy relationships. Environ Sci Technol. 44(2):650-656.
23. Liu X, Byrne RH. 1998. Comprehensive investigation of yttrium and rare earth element complexation by carbonate ions using ICP–Mass spectrometry. J Solution Chem. 27(9):803-815.
24. Hosomomi Y, Wakabayashi R, Kubota F, Kamiya N, Goto M. 2016. Diglycolic amic acid-modified *E. coli* as a biosorbent for the recovery of rare earth elements. Biochem Eng J. 113:102-106.
25. Liang CL, Shen JL. 2022. Removal of yttrium from rare-earth wastewater by *Serratia marcescens*: biosorption optimization and mechanisms studies. Sci Rep. 12(1):4861.
26. Shen JL, Liang CL, Zhong JP, Xiao MS, Zhou J, Liu J, *et al.* 2021. Adsorption behavior and mechanism of *Serratia marcescens* for Eu(III) in rare earth wastewater. Environ Sci Pollut R. 28:56915–56926.
27. Hosomomi Y, Baba Y, Kubota F, Kamiya N, Goto M, Hosomomi Y, *et al*. 2013. Biosorption of rare earth elements by *Escherichia coli*. J Chem Eng Jpn. 46(7):450-454.
28. Liu J, Zeng LQ, Liao S, Liao XF, Liu J, Mao JS, *et al*. 2020. Highly efficient enrichment and adsorption of rare earth ions (yttrium(III)) by recyclable magnetic nitrogen functionalized mesoporous expanded perlite. Chinese Chem Lett. 31(10):2849-2853.
29. Palmieri M, Volesky B, Garcia O. 2002. Biosorption of lanthanum using *Sargassum fluitans* in batch system. Hydrometallurgy. 67(1-3):31-36.
30. Hisada M, Kawase Y. 2018. Recovery of rare-earth metal neodymium from aqueous solutions by poly-γ-glutamic acid and its sodium salt as biosorbents: Effects of solution pH on neodymium recovery mechanisms. J Rare Earth. 36(05):89-97.
31. Oliveira RC, Hammer P, Guibal E, Taulemesse JM, Garcia O. 2014. Characterization of metal-biomass interactions in the lanthanum(III) biosorption on *Sargassum* sp using SEM/EDX, FTIR, and XPS: Preliminary studies. Chem Eng J. 239:381-391.
32. Maleke M, Valverde A, Vermeulen JG, Cason E, Castillo J. 2019. Biomineralization and Bioaccumulation of europium by a thermophilic metal resistant bacterium. Front Microbiol. 10:81.
33. Krishnani KK, Meng X, Christodoulatos C, Boddu VM. 2008. Biosorption mechanism of nine different heavy metals onto biomatrix from rice husk. J Hazard Mater. 153(3):1222-1234.
34. Lin ZY, Xue R, Ye YW, Zheng JH, Xu ZL. 2009. A further insight into the biosorption mechanism of Pt(IV) by infrared spectrometry. BMC Biotechnol. 9:62.
35. Roozegar M, Behnam SJEP, Energy S. 2018. An eco-friendly approach for copper (II) biosorption on alga *Cystoseira indica* and its characterization: Copper removal by alga *Cystoseira indica*. Environ Prog Sustain. 38(S1):S323-S330.
36. Sultana N, Hossain S, Mohammed ME, Irfan MF, Hossain MM. 2020. Experimental study and parameters optimization of microalgae based heavy metals removal process using a hybrid response surface methodology-crow search algorithm. Sci Rep. 10(1):15068.
37. Liu CE, Hong L, Mi NS, Liu F, Song Y, Liu ZP, *et al*. 2018. Adsorption mechanism of rare earth elements in *Laminaria ochroleuca* and *Porphyra haitanensis*. J Food Biochem. 1:12533.
38. Mishra B, Boyanov MI, Bunker BA, Kelly SD, Kemner KM, Nerenberg R, *et al*. 2009. An X-ray absorption spectroscopy study of Cd binding onto bacterial consortia. Geochim Cosmochim Ac. 73(15):4311-4325.
39. Sysoev VI, Okotrub AV, Arkhipov VE, Smirnov DA, Bulusheva LG. 2020. X-ray photoelectron study of electrical double layer at graphene/phosphoric acid interface. Appl Surf Sci. 515:146007.
40. Bertagnolli C, Uhart A, Dupin JC, Silva MGCD, Guibal E, Desbrieres J. 2014. Biosorption of chromium by alginate extraction products from *Sargassum filipendula*: Investigation of adsorption mechanisms using X-ray photoelectron spectroscopy analysis. Bioresource Technol. 164(7):264-269.
41. Ramrakhiani L, Halder A, Majumder A, Mandal AK, Majumdar S, Ghosh S. 2017. Industrial waste derived biosorbent for toxic metal remediation: Mechanism studies and spent biosorbent management. Chem Eng J. 308:1048-1064.
42. Lin LL, Starostin SA, Li SR, Khan SA, Hessel V. 2018. Synthesis of yttrium oxide nanoparticles *via* a facile microplasma-assisted process. Chem Eng Sci. 178:157-166.
43. He J, Cui A, Ni F, Deng S, Shen F, Song C, *et al.* 2019. *In situ*-generated yttrium-based nanoparticle/polyethersulfone composite adsorptive membranes: Development,

characterization, and membrane formation mechanism. J Colloid Interf Sci. 536:710–721.

44. Yu Y, Yu L, Sun M, Paul Chen J. 2016. Facile synthesis of highly active hydrated yttrium oxide towards arsenate adsorption. J Colloid Interf Sci. 474:216-222.